Nuclide production cross sections in proton-induced reactions on Bi at GeV energies

Hiroki Iwamoto[1,2,*], *Keita* Nakano[1], *Shin-ichiro* Meigo[1], *Hayato* Takeshita[1,3], and *Fujio* Maekawa[1]

[1]J-PARC Center, Japan Atomic Energy Agency, Tokai-mura, Japan
[2]Nuclear Science and Engineering Center, Japan Atomic Energy Agency, Tokai-mura, Japan
[3]Department of Advanced Energy Engineering Sciences, Kyushu University, Kasuga, Japan

Abstract. Proton-induced nuclide production cross sections for Bi at incident energies of 0.4, 1.5, and 3.0 GeV are measured with the activation method using the proton beams accelerated from the Rapid-Cycling Synchrotron of the Japan Proton Accelerator Research Complex (J-PARC). A total of 127 cross-section data are obtained. The measured data are compared with two types of Monte Carlo-based spallation models (i.e. INCL++ coupled with ABLA07 and INCL4.6 coupled with GEM), and the evaluated nuclear data library, JENDL/HE-2007. The result showed that INCL++/ABLA07 overall agrees with the experimental data, whereas INCL4.6/GEM underestimates the production of fission fragments.

1 Introduction

In the analyses of the induced radioactivity of proton accelerator facilities such as the accelerator-driven transmutation systems (ADSs) [1], spallation models to predict nuclide production in the spallation reactions or a systematic cross-section database are required. To improve the accuracy of the spallation models and evaluated nuclear reaction databases such as the JENDL high energy files [2], we are measuring the nuclide production cross sections at the Japan Proton Accelerator Research Complex (J-PARC). So far, we have acquired the nuclide production cross-section data for various targets ranging from Be (Z = 4) to Bi (Z = 83) using the J-PARC proton beams at incident energies from 0.4 to 3.0 GeV [3–9] by means of the activation method.

In this study, we measured the nuclide production cross section for Bi (^{209}Bi), which represents the major material of the ADS spallation target, at incident proton energies of 0.4, 1.5, and 3.0 GeV. The obtained cross-section data were compared with two Monte Carlo-based spallation models (i.e. the Liège intranuclear cascade (INCL) model version 4.6 [10] coupled with GEM [11] (INCL4.6/GEM) implemented in the particle and heavy-ion transport code system PHITS [12] and the INCL++ version 6.28 [13] coupled with ABLA07 [14] (INCL++/ABLA07)) and the evaluated cross-section data of the evaluated nuclear data library, JENDL/HE-2007 [2].

2 Experiment

Figure 1 shows the horizontal and vertical plane views of the J-PARC proton beamline. A target chamber was installed at a place on a beamline for beam commissioning behind the Rapid-Cycling Synchrotron (RCS) of the J-PARC [15]. This chamber was equipped with four linear guide stages with target holders on their tips (Figure 2). The Bi targets (W25 mm × H25 mm × 0.25 mm-t) were attached to three out of the four target holders, which were covered with 0.1-mm-thick Al foils. The three targets were irradiated with the 0.4-, 1.5-, and 3.0-GeV proton beams, respectively. The proton-beam current and profile were monitored using a well-calibrated current transformer and a multi-wire profile monitor, respectively. After the proton-beam irradiation, gamma-ray intensity of ra-

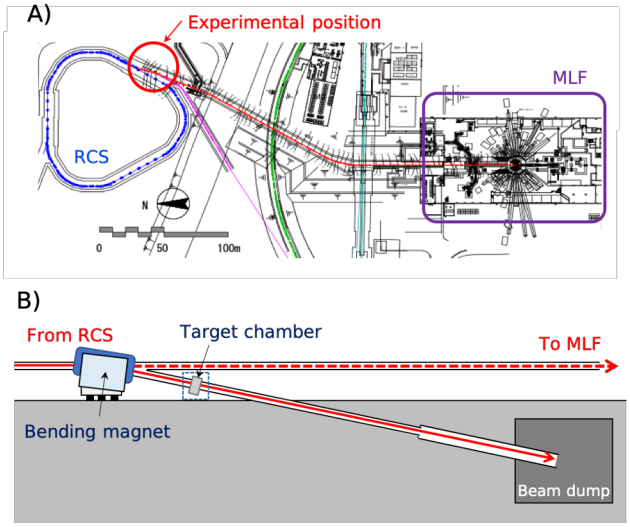

Figure 1. Horizontal and vertical plane views of the J-PARC proton beamline.

*e-mail: iwamoto.hiroki@jaea.go.jp

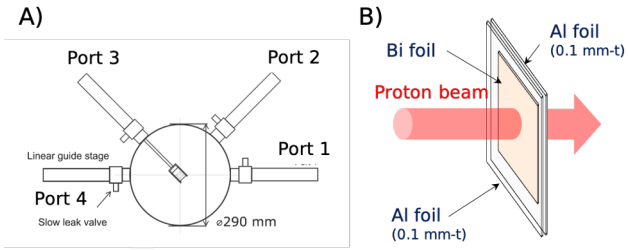

Figure 2. Target chamber (A) and Bi sample covered with Al foils (B).

dioactive nuclides produced from the irradiated samples were measured using two high-purity Germanium (HPGe) detectors (CANBERRA GC2018) via multi-channel analyzers (CANBERRA DSA-LX).

3 Derivation of cross sections

The nuclide production cross section σ was derived from the following equation:

$$\sigma = \frac{N_0}{\varsigma \hat{N}_\mathrm{p}} \quad (1)$$

where N_0 is the number of independent or cumulative product nuclides of interest, which was deduced based on gamma-ray intensity, branching ratio, detection efficiency, and radioactive decays measured using the HPGe detectors; $\hat{N}_\mathrm{p}$ is the number of incident protons, which was deduced by the following equation:

$$\hat{N}_\mathrm{p} = f_\mathrm{beam} \cdot N_\mathrm{p}, \quad (2)$$

where N_p is the number of total incident protons measured using the current transformer and f_beam is a correction factor that represents the ratio of the number of protons bombarding samples to N_p, which was obtained using an imaging plate; ς is the surface number density.

The systematic uncertainties in the measured nuclide production cross sections are listed in Table 1. Uncertainty in the gamma-ray branching ratio of each product nuclide is shown in the sixth column of Table 2. The uncertainty in the number of target nuclei was estimated based on non-uniformity of the foil thickness measured using a digital micrometer. The uncertainty in the number of incident protons was estimated based on the measurement uncertainty of the current transformer and uncertainty of the correction factor by the imaging plate. The uncertainty in the detection efficiency was obtained based on the difference between the calculated and measured results. Other possible sources of the systematic uncertainty (i.e., impurity of the target sample, the pile-up of the gamma-ray events, and inflow and outflow of the ^{24}Na between the Al and Bi foils) were negligible.

Table 1. Estimated systematic uncertainties.

	1σ uncertainty
Number of nuclei	<1%
Number of incident protons	3%
Detection efficiency	1.6%

4 Results and discussion

Table 2 summarizes the obtained nuclide production cross sections for Bi. In Table 2, types 'i' and 'c' represent independent and cumulative cross sections, respectively. In this study, we obtained a total of 127 cross-section data for 46 product nuclides and three energy points; among them, data of six nuclides (i.e. $^{202\mathrm{m}}$Pb, ^{178}Ta, $^{119\mathrm{m}}$Te, $^{120\mathrm{m}}$Sb, $^{106\mathrm{m}_1}$Ag, and ^{97}Ru) were newly acquired. Note that 61% of the data obtained were estimated to have a total uncertainty of < 5% (1σ).

Figure 3 shows comparisons of the obtained cross-section data with the INCL4.6/GEM and INCL++/ABLA07 model calculations, and the evaluated data of JENDL-HE/2007. As shown in Figure 3, INCL++/ABLA07 gives fairly good agreement with the measured data for wide mass and charge ranges, except for some isotopes. As an example of the disagreement, the ^{203}Hg production cross section is shown in the left panel of Figure 4. While the INCL4.6 calculation agrees with the measured data for Z = 83–58, which are predominantly produced from the evaporation in the de-excitation process, underestimation is seen in those for Z = 56–21; these products represent fission fragments produced from the nuclear fission in the de-excitation process. This result is similar to those of earlier benchmark results in Iwamoto et al. [16]. An illustration of the underestimation can be seen in the right panel of Figure 4. For Z = 83–58, the JENDL/HE-2007 does not reproduce the measured data very well compared to INCL++/ABLA07 and INCL4.6/GEM. As seen in Figure 4, in most cases, the obtained cross sections appear to be consistent with measurement results by Titarenko et al. [17] and Michel et al [18].

5 Conclusion

We have measured nuclide production cross sections in proton-induced reactions on Bi at incident energies of 0.4, 1.5, and 3.0 GeV at J-PARC. In this experiment, we have obtained a total of 127 cross-section data with a high degree of accuracy; 61% of the data obtained were estimated to have a total uncertainty of < 5% (1σ).

The data and findings from this study would be useful for the elucidation of spallation reaction mechanism and the improvement of spallation models. Furthermore, as addressed by Iwamoto [19], the data obtained at J-PARC are expected to be good training data in estimating the cross sections using machine learning. Thus, we will continue the nuclide production cross-section measurements.

References

[1] T. Sugawara et al., Prog. Nucl. Energy **106**, 27–33 (2018).

Table 2. Measured nuclide production cross sections. Numbers in the parentheses indicate 1σ total uncertainty.

No.	Product	Z	$T_{1/2}$	E_γ* [keV]	δI_γ† [%]	Type	Cross section (1σ uncertainty) [mb]		
							E_p = 0.4 GeV	E_p = 1.5 GeV	E_p = 3.0 GeV
1	^{207}Po	84	5.8 h	992.39	2.2	c	9.58 (0.39)	3.18 (0.13)	3.54 (0.15)
2	^{206}Po	84	8.8 h	807.38	2.3	c	10.0 (0.4)	3.55 (0.15)	3.82 (0.16)
3	^{205}Bi	83	15.31 d	1764.3	2.2	c	54.8 (2.2)	29.4 (1.2)	30.0 (1.2)
4	^{202m}Pb	82	3.54 d	422.12	6.0	c	20.7 (1.4)	11.3 (0.8)	10.1 (0.7)
5	^{202}Tl	81	12.31 d	439.51	1.1	i	6.54 (0.23)	5.35 (0.19)	5.28 (0.19)
6	^{203}Hg	80	46.594 d	279.20	0.1	c	0.228 (0.009)	0.878 (0.030)	1.82 (0.06)
7	^{196}Au	79	6.1669 d	355.73	3.4	i	0.595 (0.029)	0.791 (0.038)	0.810 (0.004)
8	^{185}Os	76	93.6 d	646.12	3.8	c	14.2 (0.7)	23.7 (1.2)	16.5 (0.8)
9	^{183}Re	75	70.0 d	162.33	8.8	c	8.19 (0.77)	18.5 (1.7)	14.7 (1.4)
10	^{181}Re	75	19.9 h	365.50	12.5	c	—	14.2 (1.8)	10.3 (1.3)
11	^{178}Ta	73	2.36 h	426.36	3.1	c	55.1 (2.54)	22.8 (1.1)	18.3 (0.8)
12	^{176}Ta	73	8.09 h	1159.3	7.3	c	8.20 (0.66)	18.5 (1.5)	14.7 (1.2)
13	^{170}Hf	72	16.01 h	164.71	26.9	c	—	20.5 (5.6)	15.4 (4.2)
14	^{171}Lu	71	8.247 d	739.79	2.7	c	0.941 (0.041)	24.1 (1.0)	16.3 (0.7)
15	^{170}Lu	71	2.012 d	1280.3	5.1	c	1.03 (0.11)	30.0 (1.8)	22.2 (1.4)
16	^{169}Lu	71	1.4197 d	191.22	3.2	c	1.45 (0.07)	17.9 (0.8)	13.8 (0.6)
17	^{169}Yb	70	32.018 h	197.96	0.3	c	0.0764 (0.0123)	18.1 (0.6)	14.4 (0.5)
18	^{153}Tb	65	2.34 d	212.00	5.8	c	—	7.71 (0.52)	11.2 (0.8)
19	^{149}Gd	64	9.28 d	149.74	6.3	c	—	7.24 (0.52)	12.6 (0.9)
20	^{147}Gd	64	1.5858 h	929.01	6.0	c	—	7.47 (0.51)	12.7 (0.9)
21	^{147}Eu	63	24.1 h	677.52	3.3	c	—	8.90 (0.42)	15.7 (0.7)
22	^{145}Eu	63	5.93 d	653.51	6.0	c	—	4.89 (0.34)	10.0 (0.7)
23	^{139}Ce	58	137.63 d	165.86	0.0	c	0.161 (0.006)	2.85 (0.10)	10.1 (0.3)
24	^{131}Ba	56	11.5 d	123.80	1.0	c	0.188 (0.010)	1.22 (0.04)	5.47 (0.19)
25	^{127}Xe	54	36.346 d	202.86	1.7	c	0.716 (0.027)	1.89 (0.07)	8.15 (0.31)
26	^{121}Te	52	19.174 d	507.59	2.8	c	2.13 (0.11)	2.43 (0.11)	7.44 (0.33)
27	^{119m}Te	52	4.7d	1212.7	0.5	c	0.314 (0.011)	0.595 (0.021)	1.42 (0.05)
28	^{124}Sb	51	60.20 d	1691.0	1.5	i	0.186 (0.008)	0.156 (0.007)	0.213 (0.009)
29	^{120m}Sb	51	5.76 d	1023.1	7.5	c	0.736 (0.061)	0.441 (0.036)	0.347 (0.029)
30	^{106m1}Ag	47	8.28 d	450.98	2.5	c	0.508 (0.024)	1.11 (0.05)	1.80 (0.08)
31	^{105}Rh	45	14.73 d	318.90	3.1	c	7.75 (0.36)	5.28 (0.24)	5.92 (0.28)
32	^{97}Ru	44	2.83 d	215.70	0.0	c	—	1.87 (0.07)	2.17 (0.08)
33	^{96}Tc	43	4.28 d	812.54	3.7	i	0.830 (0.042)	1.81 (0.09)	2.08 (0.10)
34	^{89}Zr	40	3.267 d	909.15	0.0	c	1.27 (0.04)	3.28 (0.11)	4.31 (0.15)
35	^{88}Zr	40	83.4 d	392.87	0.0	c	0.506 (0.017)	2.21 (0.08)	5.16 (0.18)
36	^{88}Y	39	106.626 d	1836.1	0.3	c	2.91 (0.10)	4.67 (0.16)	4.16 (0.14)
37	^{85}Sr	38	64.849 d	514.00	4.2	c	1.44 (0.08)	3.93 (0.21)	4.72 (0.25)
38	^{83}Rb	37	86.2 d	520.40	6.7	c	1.69 (0.13)	4.48 (0.34)	5.34 (0.40)
39	^{75}Se	34	119.78 d	264.66	0.7	c	0.398 (0.014)	1.98 (0.07)	3.10 (0.11)
40	^{74}As	33	17.77 d	595.83	5.1	i	0.918 (0.056)	2.56 (0.16)	2.70 (0.17)
41	^{65}Zn	30	243.93 d	1115.5	0.2	c	0.091 (0.010)	1.20 (0.04)	2.32 (0.08)
42	^{58}Co	27	70.86 d	810.76	0.0	i	0.0388 (0.0027)	0.651 (0.022)	1.48 (0.05)
43	^{59}Fe	26	44.49 d	1291.6	2.1	c	0.408 (0.017)	1.19 (0.05)	1.46 (0.06)
44	^{48}V	23	15.9735 d	1312.1	0.3	i	—	0.101 (0.005)	0.421 (0.015)
45	^{48}Sc	21	1.89583 d	1312.1	0.7	c	—	0.372 (0.014)	0.909 (0.032)
46	^{24}Na	11	14.997 h	1368.6	0.0	c	—	1.47 (0.05)	5.54 (0.19)

* Detected gamma-ray peak energy. † Relative uncertainty in gamma-ray branching ratio.

[2] Y. Watanabe et al., J. Korean Phys. Soc. **59**(2), 1040–1045 (2011).
[3] K. Nakano et al., *JAEA-Research 2021-014* (Japan Atomic Energy Agency, Tokai, 2022) p.25
[4] H. Matsuda et al., J. Nucl. Sci. Technol. **55**, 955–961 (2018).
[5] H. Matsuda et al., JPS Conf. Proc. **33**, 011047 (2021).
[6] H. Takeshita et al., JPS Conf. Proc. **33**, 011045 (2021).
[7] H. Takeshita et al., Nucl. Instr. Methods Phys. Res. **B527**, 17–27 (2022).
[8] H. Takeshita et al., Nucl. Instr. Methods Phys. Res. **B511**, 30–41 (2022).
[9] H. Matsuda et al., EPJ Web Conf. **239**, 06004 (2020).
[10] A. Boudard, Phys. Rev. C **87**, 014606 (2013).

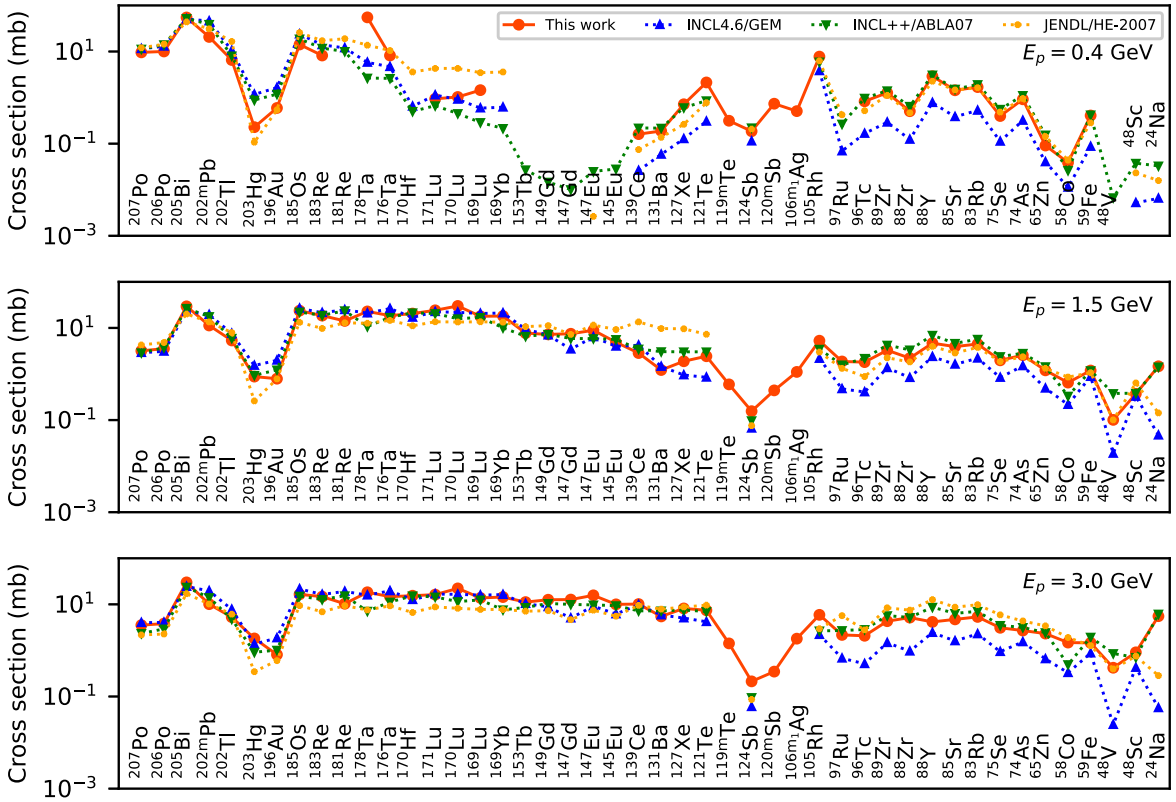

Figure 3. Nuclide production cross sections of measured product nuclides at incident proton energies of 0.4, 1.5, and 3.0 GeV, in comparison with INCL4.6/GEM, INCL++/ABLA07, and JENDL/HE-2007.

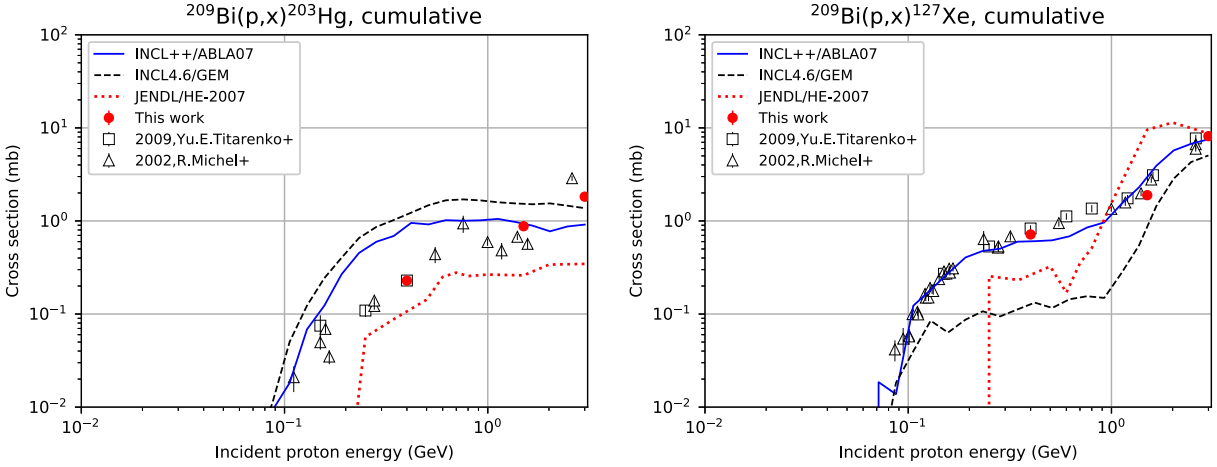

Figure 4. ^{203}Hg and ^{127}Xe production cross sections as a function of incident proton energy.

[11] S. Furihata, Nucl. Instrum. Methods Phys. Res. **B171**, 251–258 (2000).
[12] T. Sato et al. J. Nucl. Sci. Technol. **55**(5-6), 684–690 (1998).
[13] D. Mancusi et al., Phys. Rev. C. **90**, 054602 (2014).
[14] A. Kelic et al. (2009), arXiv:0906.4193.
[15] K. Yamamoto et al. J. Nucl. Sci. Technol. **59**(9), 1174–1205 (2022).
[16] Y. Iwamoto et al., J. Nucl. Sci. Technol. **54**(5), 617–635 (2017).
[17] Yu.E Titarenko et al., Technical Report of ISTC 2002, IAEA, Nuclear Data Section, Vienna, INDC(CCP)–0447, 1–692 (2009).
[18] R. Michel et al., J. Nucl. Sci. Technol. **39**(sup2), 242–245 (2002).
[19] H. Iwamoto, J. Nucl. Sci. Technol. **57**(8), 932–938 (2020).